RSC Applied Polymers

ROYAL SOCIETY OF CHEMISTRY

PAPER

View Article Online
View Journal

Cite this: DOI: 10.1039/d6lp00065g

Violacein-containing chitosan as light-sensitive, antioxidant and antibacterial hydrogels towards sustainable food packaging

Othmane Dardari,[a] Nadia Katir,[a] Mohamed Koubaa[b] and Abdelkrim El Kadib *[a,c]

Naturally derived biodegradable polymers offer sustainable alternatives to fossil-based plastics in food packaging. In this study, multifunctional packaging films were prepared by integrating biomass-derived chitosan with violacein, a biotechnologically synthesized pigment. The resulting violacein–chitosan networks formed light-responsive hydrogels that could be cast into films or applied as coatings. Successful incorporation of violacein was confirmed by FTIR and UV–Vis analyses, supported by distinct optical and photoluminescence properties. SEM imaging revealed increased surface roughness and pigment aggregation at higher violacein loadings. The water solubility decreased markedly from 72.23% for pure chitosan to 19.33% for **CS@Vio$^{10\%}$-*f***, while the water vapor permeability decreased from 8.09×10^{-9} to 4.33×10^{-9} g m (s Pa)$^{-1}$. Contact angle measurements indicated enhanced hydrophobicity, increasing from 74.3° for pristine chitosan) to 107.3° for **CS@Vio$^{10\%}$-*f***. Violocaein incorporation allows at 5% optimal loading to improve the tensile strength (56 MPa), Young's modulus (1360 MPa) and elongation at break (51%), a unique behaviour that can be rooted in the bifaceted structure of the pigment, acting simultaneously as a plasticizer and stiffening reagent. Violacein endowed also the films with remarkable UV-shielding (up to 87.8% UVA and 98.9% UVB protection) and antioxidant properties, with the radical scavenging activity reaching 75% at 10% violacein loading. Antibacterial assays showed up to 80% inhibition of *S. aureus* and 71% inhibition of *E. coli*, outperforming pristine chitosan (60% and 65%, respectively). Furthermore, the films effectively extended the shelf life of strawberries, blueberries, and raspberries. Overall, these findings highlight the potential of violacein–chitosan films as sustainable, multifunctional materials for active food packaging and preservation.

Received 25th February 2026,
Accepted 12th April 2026

DOI: 10.1039/d6lp00065g

rsc.li/rscapplpolym

Introduction

The circular economy represents a key pillar for promoting sustainable development worldwide.[1,2] Significant efforts have focused on transforming biomass and bio-waste, notably through the extensive valorization of Earth-abundant cellulose and lignin derivatives.[3–6] In contrast, the potential of marine-origin resources remains comparatively underexplored, with circularity in this sector still far from maturity.[7–13] Despite their rich chemical composition and promising properties, many discarded oceanic resources are often reintroduced into marine ecosystems along with by-catches, incinerated, or simply neglected as byproducts. Unfortunately, these practices heavily contribute to waste management challenges and aesthetic degradation, particularly in coastal and touristic areas.[14] Among these underutilized resources, crustacean waste comprising shells and other inedible fractions represents a valuable source of chitin, the second most abundant biopolymer on Earth.[15,16] This biopolymer offers great potential as a renewable building block for the development of high-performance materials, functional products, and advanced sustainable commodities.

Due to its chemical recalcitrance and insolubility in conventional solvents, chitin is commonly deacetylated to yield chitosan, an astonishing amino-polysaccharide with a wide range of valuable properties.[17,18] Consequently, chitosan has emerged as a highly attractive material for the fabrication of nanostructured films and coatings[19–22] intended for food and biomedical applications.[23–25] Despite its intrinsic advantages, pristine chitosan exhibits relatively poor mechanical strength, limited UV-shielding capacity, and only moderate biological

[a]Euromed University of Fes, UEMF, Morocco. E-mail: a.elkadib@ueuromed.org
[b]Université de Technologie de Compiègne, ESCOM, TIMR (Integrated Transformations of Renewable Matter), Centre de recherche Royallieu, CS 60 319, 60 203 Compiègne, Cedex, France
[c]Hassan II Academy of Science and Technology, Rabat, Morocco

activity.[26] These shortcomings have been partly overcome by combining chitosan with bioactive organic molecules, metal or metal oxide nanoparticles, and nanometric fillers, thereby enhancing the functional and structural performance of the resulting composites.[27,28] Hitherto, active pharmaceutical or bio-functional ingredients are incorporated through entrapment or chemical grafting onto the amine groups of chitosan, which significantly improves its biological activity.[29,30] In many cases also, the hydrophobicity and rigidity of cyclic and planar organic skeletons further contribute to reinforcing the network structure, reducing moisture sensitivity, and improving mechanical stability.[31,32] However, many of these additives are derived from petroleum-based precursors synthesized *via* conventional organic chemistry, raising concerns regarding toxicity, environmental impact, and production costs for the final packaging materials. A more sustainable approach to active packaging and coating design emphasizes the elimination of synthetic additives and the use of bio-based components, such as biomass-derived polymer matrices, naturally occurring microbial agents with antibacterial activity, and non-synthetic pigments providing photonic or sensing functionalities.[33]

In this context, we become interested in utilizing the biotechnologically engineered violacein[34] to craft multifunctional and sustainable hydrogels for coating and packaging applications. Violacein is a light-sensitive purple pigment produced *via* the enzymatic oxidation and condensation of two L-tryptophan molecules, catalyzed by a cascade of five enzymes encoded by the genes VioA, VioB, VioC, VioD, and VioE.[35] It is biosynthesized using a genetically modified *Yarrowia lipolytica* strain as a production chassis, offering a significantly lower environmental impact compared to conventional chemical synthesis and thereby aligning with the principles of green chemistry.[36] Structurally, violacein contains functional groups such as amides and hydroxyls capable of hydrogen bonding, as well as a rigid planar polyaromatic core favorable for π–π stacking interactions; all of which facilitate its stable incorporation within a polymeric network. Despite its diverse functionalities and broad benefits, including antioxidant, antibacterial, antiviral, and UV-shielding activities, its integration into natural or synthetic hydrogels has been seldom explored.[37] Herein, we report the successful association of violacein with chitosan in colloidal solutions to fabricate micrometer-thick films *via* evaporation-induced self-assembly. Our results demonstrate that up to a 10% molar ratio of violacein can be accommodated within the chitosan matrix while preserving the film-forming memory, yielding flexible, homogeneous, and transparent hybrid films. The encapsulation of violacein led to enhanced mechanical stability, antioxidant and antibacterial performance, as well as additional photoluminescence and UV-shielding properties relative to pristine chitosan films. The potential of these functional hydrogel coatings was further demonstrated through the extended preservation of perishable fruits and their ability to detect trace amounts of residual copper, highlighting their promise for sustainable food packaging, safety, and monitoring applications.

Results and discussion

Preparation and chemical characterization of the violacein-containing chitosan films

Violacein-containing chitosan hydrogel films were prepared from aqueous acidic chitosan solutions, to which a known amount of violacein dissolved in ethanol was added, yielding a series of gels with increasing violacein molar ratios of 1, 3, 5, and 10%. Upon addition, the solution became distinctly colored, consistent with the entrapment of violacein within the chitosan matrix. Transparent, flexible, and good-quality films were subsequently obtained by solvent casting in Petri dishes (Fig. 1).

The resulting films could be easily detached from the support and handled without special precautions. The incorporation of violacein did not affect the film quality or flexibility. However, a noticeable intensification of the purple coloration was observed in the **CS@Vio$^{X\%}$-*f*** films (X = 1, 3, 5, and 10%), correlating with the increasing violacein content in the precursor solution (Fig. 1). The thickness of the dried films, measured using a digital caliper, increased with the amount of incorporated violacein, from 43 μm for pristine chitosan **CS-*f*** to 91 μm for **CS@Vio$^{10\%}$-*f*** (Table S1, SI). It should be emphasized that violacein was used herein without further purification as the films are intended for food packaging and coating applications. Isolating violacein implies the use of organic solvents that are not compatible with food chemistry.[38] Besides, the use of crude extracts significantly reduces production costs and maintains sufficient antimicrobial and antioxidant activities for industrial use.

FTIR analysis of the pristine chitosan films reveals characteristic peaks including a broad band at around 3311 cm^{-1} (O–H stretching), a peak at 2922 cm^{-1} (C–H stretching), and signals at 1642, 1532, and 1020 cm^{-1}, corresponding to the C═O, N–H, and C–O–C stretching, respectively (Fig. S1). FTIR of the violacein alone displays broad bands between 3000 and 3600 cm^{-1} assignable to the overlap of O–H and N–H stretching, as well as the NH(C═O) peak at 1637 cm^{-1}, the C–N stretching at 1245 cm^{-1}, the C–O stretching of phenol at 1024 cm^{-1}, and aromatic C–H out-of-plane deformations from 500 to 700 cm^{-1}. FTIR spectra of violacein-embedding chitosan films show mainly the fingerprint of the holding chitosan polymer as described above, with minor alteration caused by the appearance of the violacein signature or because of its interplay with chitosan. For instance, a marginal alteration of the pattern of the O–H region (3000–3600 cm^{-1}) was observed, due to the presence of abundant portion of NH groups from violacein, creating an additional hydrogen-bonding network. Also, a slight decrease in the N–H peak at 1532 cm^{-1} accompanied by a marginal shift was noticed with increasing violacein concentration, which could suggest the occurrence of weak hydrogen bonding or electrostatic interactions involving the glucosamine units of chitosan with polar functional groups of the violacein backbone. The appearance of the C–H peak at 2922 cm^{-1} reflects an increase in the concentration of alkyl groups in violacein-containing films. Furthermore, the

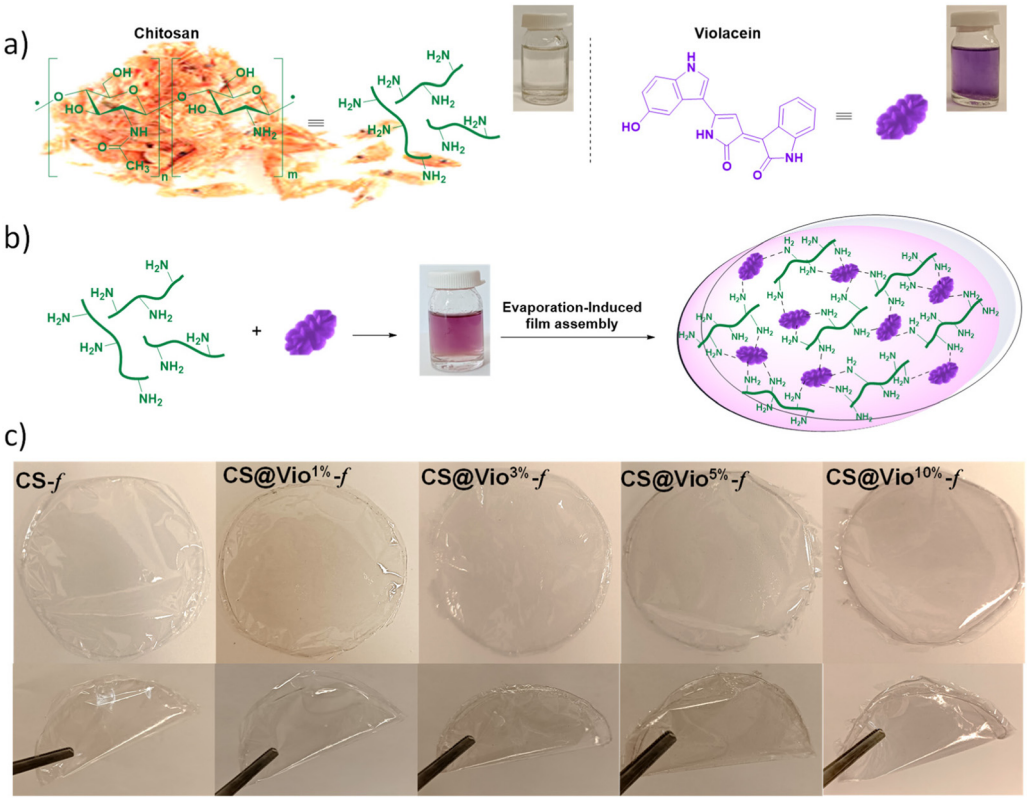

Fig. 1 Multistep preparation of violacein-containing chitosan **CS@Vio$^{X\%}$-*f*** films. (a) Chemical structure of chitosan and violacein and their respective solution. (b) Plausible interplay of violacein and chitosan within the network. (c) Digital photos of the cast violacein-containing chitosan **CS@Vio$^{X\%}$-*f*** films (X = 0, 1, 3, 5 and 10%) with X reflecting the molar ratio of violacein with respect to NH_2 groups belonging to chitosan.

aromatic structure of violacein around 591 cm^{-1} becomes ostensible for the 5% and 10% violacein-containing chitosan films.

Structural and textural characterization of the violacein-containing chitosan films

The consequence of the entrapment of violacein inside of the biopolymer was moreover investigated using X-ray diffraction (XRD), scanning electron microscopy (SEM), and water contact angle measurement. The XRD pattern of native chitosan film displays only broad peaks, consistent with its amorphous nature (Fig. S2). The XRD patterns of pure violacein shows several distinct peaks at 2θ = 8.5°, 21.25°, and 27.5°, indicating a well-defined crystalline structure, consistent with the previous literature.[39,40] Regardless the loaded violacein amount inside the films, none of **CS@Vio$^{X\%}$-*f*** reveal the above-mentioned crystalline peaks. This points to the disturbance of periodical ordering inside of the film-forming network, thereby reflecting a great molecular dispersion of violacein within the matrix owing to the strong interfacial interaction occurring through hydrogen bonding between violacein and chitosan chains.

SEM images of native chitosan film reveal a smooth and homogeneous surface, as the slow solvent evaporation process promotes strong hydrogen bonding between chitosan chains, forming a dense and ordered network.[41,42] When violacein is introduced into the film-forming solution, the surface morphology undergoes notable changes. At lower concentrations (1% and 3% violacein), minor roughness and very few aggregated particles appear, but the network remains relatively continuous, suggesting that the chitosan matrix can accommodate their supramolecular ordering without significant disruption. However, from 5% violacein upwards, significant aggregation occurs, leading to an increase in surface roughness. At 10%, SEM images reveal even larger and more pronounced aggregates of violacein. These aggregates suggest that violacein is predominantly packed within the film-forming solution, and disrupting this packing requires increasing amounts of energy. This concentration-dependent aggregation has already been observed in many previous reports.[43] As will be commented later, this packing-induced aggregation has a detrimental effect on the barrier and mechanical properties of the resulting films. Thus, violacein-containing chitosan films evolve from a homogeneous micrometer-thick layer to an irregular and discontinuous network, highlighting the challenges of dispersing violacein pigment at high concentrations inside the hydrogen-bonded polymeric network of the chitosan matrix.

Water contact angle measurements show a gradual increase corresponding to the increasing incorporation of violacein into the films (Fig. 2, inset). Pristine chitosan film displays a

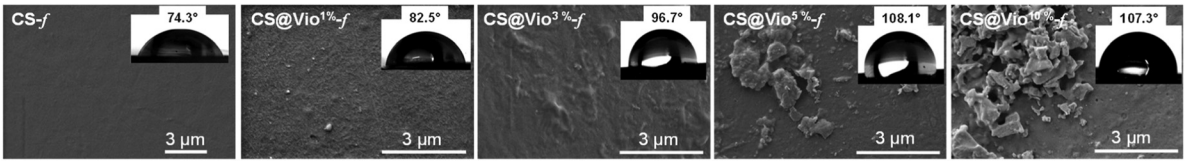

Fig. 2 Scanning electron microscopy and water contact angle measurements (inset) of **CS@Vio$^{X\%}$-*f*** films (X = 0, 1, 3, 5 and 10%).

relatively low contact angle value of 74.3°, typical of a carbohydrate-based hydrophilic surface. This is due to the presence of hydroxyl and amine functional groups on chitosan, which promote hydrogen bond formation with water molecules, thereby increasing their interaction.[44] Upon addition of 1% violacein, the contact angle rises to 82.5°, indicating a decrease in water affinity and an increase in hydrophobicity. This trend further continues with contact angles of 96.7° for film-containing 3% violacein and 108.1° for those incorporating 5% of violacein, plausibly reaching a plateau upon incorporating 10% of violacein, resulting in a contact angle value of 107.3°. This increase can be explained by the hydrophobic character of violacein,[45] which once incorporated into the chitosan matrix, modifies the surface structure of the film by exposing its rigid and planar ring, thereby limiting the interaction of chitosan's hydrophilic groups with water. At higher loading, violacein is likely to form a more extended layer on the surface, probably through π–π stacking, resulting in an increased hydrophobic effect.

Water-related, thermal and mechanical properties of the violacein-containing chitosan films

Further investigation into the water-related behavior reveals that the incorporation of violacein into chitosan films results in a progressive decrease in water solubility (WS) with increasing violacein concentration (Fig. 3a). The WS decreases from 72.23% for pure chitosan to 53% and 40.33% at 1% and 3% violacein, respectively. At higher concentrations, specifically 5% and 10%, the WS further decreases to 34.67% and 19.33%. This reduction can be attributed to the hydrophobic nature of violacein[46] and its entanglement within the biopolymer network, which induces a crosslinking-like effect. In terms of water vapor permeability (Fig. 3b), the addition of violacein also leads to a gradual reduction at low concentrations (1% and 3%). At these levels, violacein is uniformly incorporated into the polymer network, slightly densifying the film without significantly disrupting its structure. This integration slows down, yet regulates, water vapor diffusion, reducing the WVP from 8.09 × 10^{-9} g m^{-1} s^{-1} Pa^{-1} for pure chitosan to 6.11 × 10^{-9} and 4.33 × 10^{-9} g m^{-1} s^{-1} Pa^{-1} at 1% and 3%, respectively. This reduction is attributed to the homogeneous dispersion of violacein, which renders the film more compact and less permeable. However, at concentrations above 5%, violacein begins to aggregate, altering the film texture. For **CS@Vio$^{5\%}$-*f*** and **CS@Vio$^{10\%}$-*f***, the WVP values increase slightly to 4.75 × 10^{-9} and 4.97 × 10^{-9} g m^{-1} s^{-1} Pa^{-1}, respectively. This suggests that beyond 5% loading, violacein molecules tend to self-associate through π–π stacking, disrupting the homogeneous distribution and creating additional diffusion pathways that facilitate water vapor transmission.

Thermogravimetric analyses (TGA) of native **CS-*f*** and modified **CS@Vio$^{3\%}$-*f*** and **CS@Vio$^{10\%}$-*f*** films reveal distinct thermal behavior as a consequence of violacein incorporation (Fig. S3). During the first stage (from room temperature to 120 °C), the reduced mass loss observed for the modified films indicates a decrease in water adsorption, probably due to the hydrophobic nature of violacein, which reduces the film's sensitivity to moisture. The second stage (120–400 °C) corresponds to the main thermal degradation of the chitosan skeleton. Above 400 °C, the modified films do not show a distinct third degradation stage, compared to native chitosan films, suggesting a suppression of the late decomposition. The higher residual mass observed for **CS@Vio$^{10\%}$-*f*** compared with **CS-*f*** further confirms the improved thermal stability of films with a high violacein content.

Mechanical properties were next studied to assess the influence of increased violacein on the nanocomposite films (Fig. 4). At the first glance, both the tensile modulus and tensile strength of the films showed a marked increase with the addition of violacein (Fig. 4a and b). While pristine CS film displays a tensile strength of 41 MPa, the use of 1% of violacein increases the tensile strength to 45 MPa. A maximum tensile strength of 56 MPa was further reached with 5% violacein, but at a higher violacein concentration of 10%, the tensile strength decreases slightly to 54 MPa. This suggests that above a certain threshold, tactoid-like aggregated violacein particulates induce some structural instability into the matrix. The Young's modulus of the films reveals slight variations, with values increasing slightly from 1204 MPa for pristine chitosan films to 1360 MPa for **CS@Vio$^{5\%}$-*f***, indicating that violacein incorporation significantly improves the film stiffness

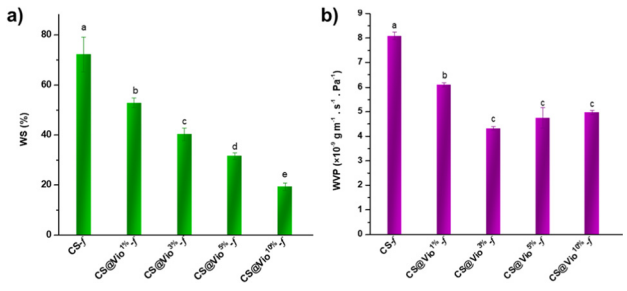

Fig. 3 (a) WS and (b) WVP of **CS@Vio$^{X\%}$-*f*** films (X = 0, 1, 3, 5 and 10%).

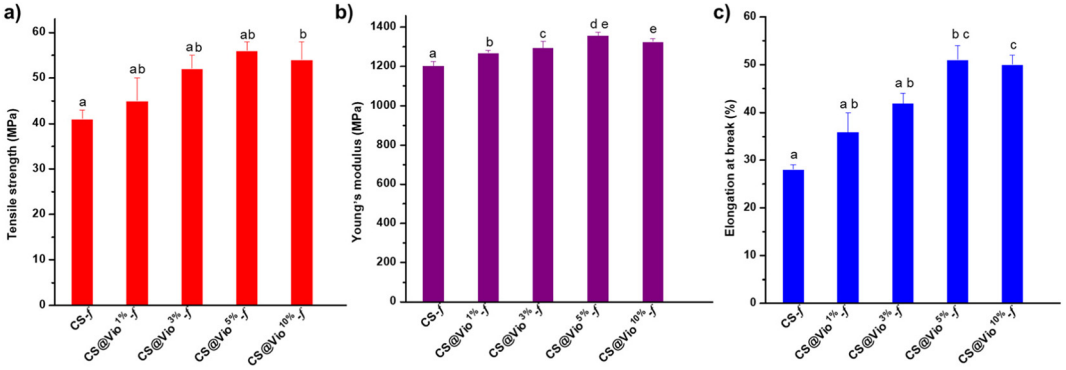

Fig. 4 Mechanical properties of **CS@Vio$^{X\%}$-*f*** with (X = 0, 1, 3, 5 and 10%). (a) Young modulus, (b) tensile strength, and (c) elongation at break.

(Fig. 4a). However, at the highest concentration of violacein (10%), the modulus drops slightly to 1326 MPa, suggesting that at this concentration, the aggregated state of the violacein results in a slight decrease in stiffness. This scenario is reminiscent of the use of montmorillonite clay particulates, where individual exfoliated clay sheets bring generally improved tensile strength and Young's modulus, while intercalated or aggregated particles are rather detrimental for the mechanical stability.[47,48] In terms of elongation at break, the incorporation of violacein considerably improves the network flexibility (Fig. 4c). The pristine CS film records a modest elongation of 28%, but a progressive improvement was noticed as the violacein content increases, reaching 51% for the **CS@Vio$^{5\%}$-*f*** film. This increase in elongation suggests that violacein acts as a plasticizer, allowing greater flexibility without compromising the tensile strength too much.[37] The improvement of the three antagonistic parameters at the same time could be attributed to the simultaneous presence in violacein of hydrogen-donating groups that account for its role as a plasticizer and the planar rigid network that improves the stiffness of the films.

Optical properties of the violacein-containing chitosan films

The color parameters (L^*, a^*, b^*) of the chitosan and violacein-reinforced films were analyzed using a DataColor spectrophotometer. The results revealed a clear and progressive change in color intensity with increasing violacein content (Table 1). The L^* values decreased markedly from 88.2 for the pure chitosan film (**CS-*f***) to 29.0 for **CS@Vio$^{10\%}$-*f***, indicating a gradual darkening of the films. Concurrently, the a^* (red–green) values increased from 2.6 to 10.5, reflecting a shift toward red tones, while the b^* (yellow–blue) values remained negative, from −11.6 to −6.3, confirming the persistence of a blue component. The combination of increasing red (a^*) and stable blue ($-b^*$) hues resulted in the characteristic violet coloration of violacein-containing films. The overall color difference (ΔE) increased proportionally with violacein concentration, confirming efficient pigment incorporation. These results demonstrate that violacein effectively alters the optical properties of chitosan films, producing increasingly intense violet shades as its concentration rises.

The light-sensitivity of the violacein backbone prompted us to investigate UV-visible and photoluminescence properties of the final hydrogel films (Fig. 5). In ethanol solution, UV-visible spectra of violacein display an absorption peak with a maximum wavelength at around λ = 566 nm and two others at λ = 352 nm and λ = 268 nm (Fig. 5a, left). The former bond is due to the presence of highly conjugated indole and oxindole moieties that are responsible for its distinctive violet color[49] through the electronic transition from π to π* orbitals.[50] The second and the third one are associated with charge transfer within the conjugated rings of violacein.[51] Violacein-containing chitosan films display an absorption peak at around λ = 578 nm, with the corresponding intensity being correlated with the loaded amount of violacein inside the films (Fig. 5b, left). The bathochromic shift in the maximum wavelength of violacein-containing films *versus* the one in solution ($\Delta\lambda$ = 12 nm) could be related to the alteration of the violacein conformation upon confinement or the occurrence of strong hydrogen bonding with the biopolymer network. When the solution of violacein in ethanol is excited at 402 nm, it emits

Table 1 Color parameters (L^*, a^*, b^*, ΔE) of **CS@Vio$^{X\%}$-*f*** (X = 0, 1, 3, 5 and 10%)

Films	L^*	a^*	b^*	ΔE
CS-*f*	88.2 ± 0.21^{a}	2.6 ± 0.01^{a}	−11.6 ± 0.01^{a}	—
CS@Vio$^{1\%}$-*f*	74.5 ± 0.04^{b}	4.6 ± 0.03^{b}	−12.5 ± 0.03^{bd}	14.3 ± 0.02^{a}
CS@Vio$^{3\%}$-*f*	61.5 ± 0.3^{c}	8.4 ± 0.03^{c}	−13.6 ± 0.06^{c}	27.6 ± 0.03^{b}
CS@Vio$^{5\%}$-*f*	50.5 ± 0.01^{d}	11.5 ± 0.01^{d}	−12.4 ± 0.01^{d}	39.2 ± 0.01^{c}
CS@Vio$^{10\%}$-*f*	29 ± 0.57^{e}	10.5 ± 0.02^{e}	−6.3 ± 0.02^{e}	62.7 ± 0.01^{d}

The values in the same column followed by the same letter are not significantly different ($p < 0.05$).

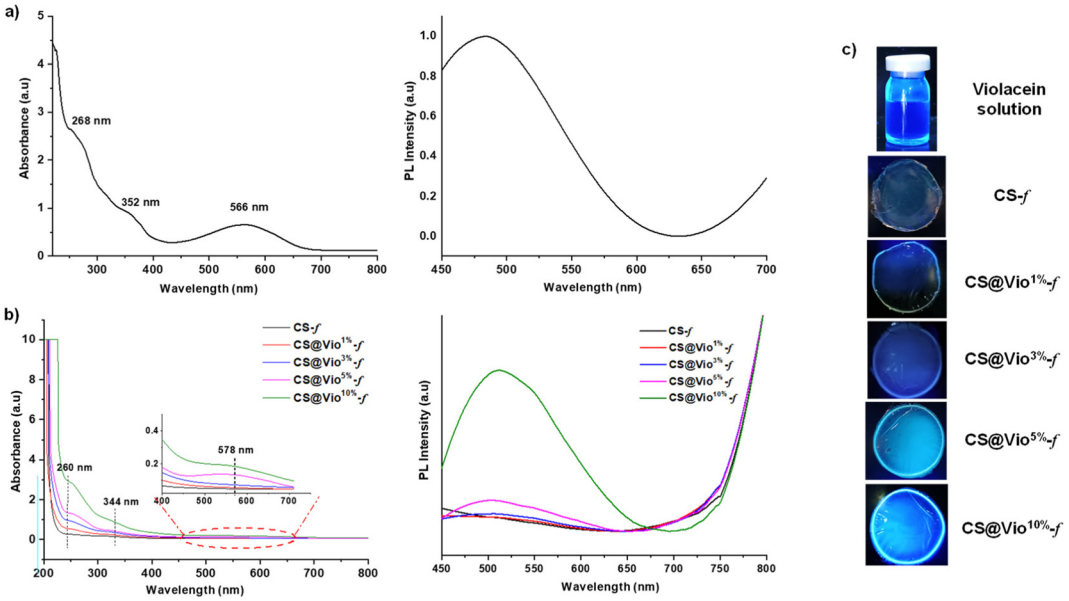

Fig. 5 Optical properties: (a) UV-Vis and photoluminescence of violacein solution in ethanol (C = 5.8 10^{-3} mol l^{-1}). (b) UV-Vis and photoluminescence of **CS@Vio$^{X\%}$-*f*** films (X = 0, 1, 3, 5 and 10%). (c) Digital photographs of violacein in solution and violacein-containing films.

light at a specific wavelength of 483 nm (Fig. 5a, right). This emission corresponds to the relaxation of electrons in the violacein molecule, releasing energy in the form of light at a specific wavelength.[52,53] In violacein-containing chitosan films, such emission is rather observed at 510 nm, being indeed shifted by nearly 25 nm (Fig. 5b, right). The intensity of the emission peak parallels the increase of violacein loading, reflecting an increased density of excitable molecules in the film. The remarkable amplification seen for **CS-Vio$^{10\%}$-*f*** could be associated with the formation of extended chromophore species (ex. excimers), owing to the significant stacking and supramolecular interaction of different violacein units incorporated within the films. This is consistent with the findings from the SEM analysis and mechanical studies.

Given the high absorbance of the violet-colored violacein pigment in the UV range, attributed to its π-conjugated resonance structure, we envisioned that violacein-containing chitosan films can selectively absorb UV radiation and protect food from spoilage caused by this radiation. The detrimental effect of UVA (315–400 nm), UVB (280–315 nm) and UVC (200–280 nm) rays on food is well established as they can penetrate and degrade products by altering their nutrients, colors, textures and flavors, as well as accelerating the rancidity and oxidation processes.[54,55] A significant reduction in UV transmittance was noticed for **CS@Vio$^{X\%}$-*f*** compared to pristine chitosan films (Fig. S5 and S6, SI). UVA and UVB protection rates increased with increasing violacein content within the films (Fig. S5, SI). For example, **CS@Vio$^{10\%}$-*f*** film offers protection rates of 87.8% and 98.9% for UVA and UVB radiation, respectively, demonstrating exceptional blocking ability compared to pristine chitosan films, which only protect against 22.9% of UVA and 36.8% of UVB radiation (Table S1, SI). At visible wavelengths of T_{660}, the pristine chitosan film showed the greatest clarity with a transmittance of 89.43% (Fig. S6, SI). In turn, **CS@Vio$^{X\%}$-*f*** films showed progressively lower transparency with increasing violacein loading inside, being equal to 85.54% for **CS@Vio$^{10\%}$-*f*** (Table S1, SI). Despite this increase in opacity, the films remained sufficiently transparent and visible. The decrease in transparency correlates with the film thickness that increases from 43 μm for pristine chitosan films to 91 μm for **CS@Vio$^{10\%}$-*f*** (Table S1, SI). As a result, **CS@Vio$^{10\%}$-*f***, displaying the highest violacein loading, offers superior UV protection with a slight alteration of its transparency, making it suitable for applications requesting UV protection and reduced light transmission.[56]

Antioxidant activity and total phenolic content of the violacein-containing chitosan films

The antioxidant activity has been next investigated for native chitosan and violacein-containing chitosan films using the DPPH method (Fig. 6a). Pristine chitosan films display a moderate anti-

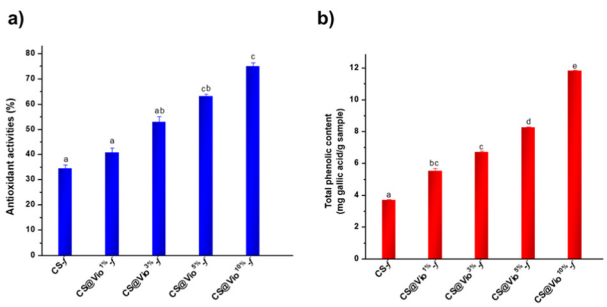

Fig. 6 (a) Antioxidant activity and (b) total phenolic content of **CS@Vio$^{X\%}$-*f*** films (X = 0, 1, 3, 5 and 10%), using the DPPH and F–C methods, respectively.

oxidant activity of 35%, contrasting with greater antioxidant activity of 41%, 53%, 63% and 75% recorded respectively for films containing 1%, 3%, 5% and 10% violacein. The ability of violacein to effectively act against free radicals could be explained by its hydrogen-donating properties, as well as the low dissociation energy of its N–H bonds compared with those of DPPH.[57,58] The increased efficacy of the films with increasing concentration of violacein confirms the pivotal role of the latter in neutralizing free radicals, which is expected to stimulate the development of new biocompatible materials enriched with antioxidants for food packaging and coating medical devices. However, it is important to note that the DPPH assay alone does not fully capture the complexity of antioxidant mechanisms, as it primarily measures free radical scavenging activity. This limitation underscores the need for additional antioxidant assays to provide a more comprehensive evaluation. For instance, the total phenolic content test (TPC) could be used to confirm this, as it measures the phenolic content, supporting the hypothesis that violacein contains phenolic compounds. This can be carried out using the Folin–Ciocalteu (F–C) colorimetric method (Fig. 6b). Pure chitosan film (**CS-*f***), known for its negligible content of phenolic compounds,[59] exhibited a very low TPC value of 3.6 mg GAE g^{-1}. Upon incorporation of violacein, a gradual increase in TPC was observed, reaching a maximum of 12 mg GAE g^{-1} for **CS@Vio$^{10\%}$-*f***. This enhancement suggests that violacein contributes to the apparent phenolic content within the chitosan matrix. Although violacein is thought to contain phenolic-like moieties, its precise phenolic contribution remains poorly documented in the literature, particularly when compared with conventional phenolic sources such as plant extracts or essential oils. Additionally, as *Y. lipolytica* is known for its ability to produce phenol-degrading enzymes, and the Folin–Ciocalteu reagent may also react with other metabolites like aromatic amino acids and peptides, further studies are needed to accurately assess the specific phenolic contribution of violacein in this system.

Antibacterial activity of the violacein-containing chitosan films

The antibacterial properties of chitosan-based films against foodborne pathogens *E. coli* and *S. aureus* were examined by two complementary methods (Fig. 7, Table 2 and Fig. S7). The control sample, under film-free conditions, demonstrated a noticeable increase in bacterial growth for both pathogens after 24 hours of incubation. However, the use of pristine or modified chitosan films prevented bacterial growth. Specifically, the pristine chitosan film resulted in a reduction of *S. aureus* and *E. coli* colonies compared to the control, from approximately 4.6 to 3.86 and from 4.2 to 3.17 in log (CFU mL^{-1}) respectively after 24 hours. This reduction is attributed to the interaction between the cationic chitosan and the negatively charged lipopolysaccharides of the bacterial cell membrane, which increases the membrane permeability, leading to leakage of intracellular components.[60]

Additionally, chitosan's ability to chelate essential environmental ions and nutrients disrupts the bacterial cell wall and membrane.[61,62] The antimicrobial properties of chitosan have been debated, but it is generally more effective against Gram-negative bacteria due to differences in cell wall composition.[63,64] The incorporation of bioactive violacein into chitosan films significantly enhanced their antibacterial activity against both Gram-negative and Gram-positive bacteria.[65] This effect was concentration dependent, with higher violacein concentrations correlating with greater antibacterial activity. For instance, **CS@Vio$^{1\%}$-*f*** and **CS@Vio$^{10\%}$-*f*** films reduced *S. aureus* colony counts from 4.6 to 3.69 and 1.16 in log (CFU mL^{-1}), respectively, and *E. coli* colony counts decreased from 4.2 to 3.1 and 2.2 in log (CFU mL^{-1}). These findings indicate that violacein-containing chitosan films significantly inhibited *S. aureus*, though the effect on *E. coli* was

Table 2 Inhibition of the bacterial growth zone of chitosan-based films against *S. aureus* and *E. coli* bacteria using the disk diffusion method

	Inhibition zone (mm)	
Films	*E. coli*	*S. aureus*
CS-*f*	1.2 ± 0.2^{a}	1.4 ± 0.1^{a}
CS@Vio$^{1\%}$-*f*	1.4 ± 0.08^{a}	1.6 ± 0.08^{b}
CS@Vio$^{3\%}$-*f*	1.7 ± 0.1^{b}	1.9 ± 0.14^{c}
CS@Vio$^{5\%}$-*f*	1.8 ± 0.01^{b}	2.1 ± 0.1^{d}
CS@Vio$^{10\%}$-*f*	2 ± 0.05^{c}	2.5 ± 0.2^{e}

Letters (a, b, c) are used to show which group means are statistically different from others (same letter = no difference).

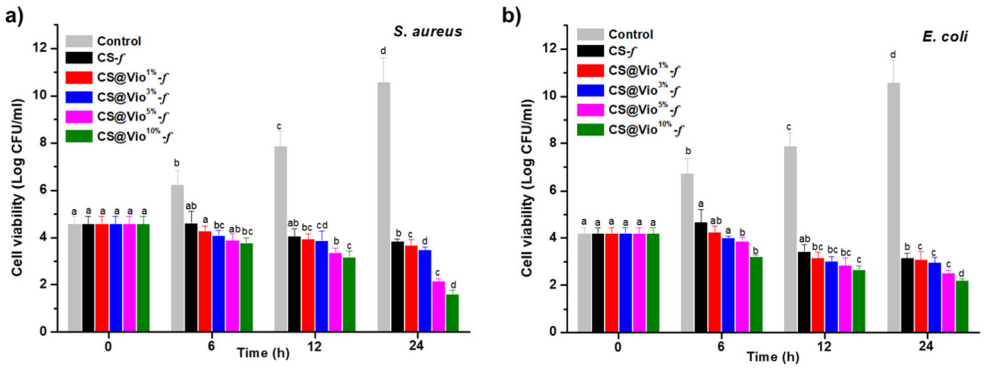

Fig. 7 Antibacterial activities of **CS@Vio$^{X\%}$-*f*** (X = 0, 1, 3, 5 and 10%) against (a) Gram-positive bacteria (*S. aureus*) and (b) Gram-negative bacteria (*E. coli*) using the total viable colony count method.

less pronounced, consistent with the stronger action of violacein against Gram-positive bacteria as previously reported.[66,67] In terms of inhibition, **CS@Vio$^{10\%}$-*f*** achieved nearly 80% growth inhibition of *S. aureus* and 71% inhibition of *E. coli*, compared to 60% and 65% inhibition observed with pristine chitosan films. These results align with the inhibition zone data presented in Table 2 and Fig. S7b. The inhibition zones increased with higher violacein concentrations, with **CS@Vio$^{1\%}$-*f*** showing zones of 1.4 mm and 1.6 mm, respectively, for *E. coli* and *S. aureus*, where the **CS@Vio$^{10\%}$-*f*** films achieved the largest inhibition zones of 2.0 mm for *E. coli* and 2.5 mm for *S. aureus*. The inhibition zones and the reduction in viable colony counts indicate that violacein's antibacterial activity is enhanced when incorporated into the chitosan matrix.[68] Achieving this antibacterial performance is appealing considering that the tested films do not contain commonly used metal nanoparticles (*e.g.*, silver, copper, gold) and are made entirely from sustainable, cost-effective and biodegradable materials.[69,70]

Food packaging application

Given the well-established antibacterial and antifungal properties of violacein extracts along with the film-forming ability of chitosan, we preliminarily investigated the potential use of the resulting hydrogels as a protective edible coating for extending the shelf-life of fruits and vegetables, aiming to provide an effective barrier against moisture exchange and to act as a bulwark against microbial growth.[71] A comparative study was consequently conducted using pristine chitosan **CS-s**, pure violacein **Vio-s** as well as **CS@Vio$^{10\%}$-s** film-forming solution (s stands for solution). Three representative perishable fruits, including strawberries, blueberries and raspberries, were selected for this purpose (Fig. S8, SI). Visual observation revealed that the uncoated strawberries showed signs of deterioration, manifested by darkening of the skin and the appearance of mold as early as day five. Strawberries are particularly susceptible to damage caused by vibration during transportation, which can lead to abrasions and bruising. This damage allows microbes to penetrate, leading to fruit degradation and reduced shelf life.[72] In contrast, samples coated with **CS-s**, **Vio$^{10\%}$-s** and **CS@Vio$^{10\%}$-s** show complete deterioration at 10 days. For raspberries, all samples were damaged by day 5, showing no significant improvement in preservation. The control group showed rapid ripening, while those coated with chitosan, violacein, or **CS@Vio$^{10\%}$-s** exhibited similar signs of deterioration by day 5. It should be noted that raspberries are extremely perishable due to their high moisture content, high respiration rate and delicate structure, making them particularly susceptible to physical damage and spoilage.[73] For blueberries, coated with **CS@Vio$^{10\%}$-s**, samples retained their shape and resisted physical degradation for over ten days, while uncoated samples showed signs of deterioration after ten days. These results can be explained by several complex mechanisms. Firstly, **CS@Vio$^{10\%}$-*s*** based coatings form a stable colloidal solution with more suitable rheological properties, owing to the chemical interplay between violacein and chitosan. This optimized formulation can generate a more effective protective barrier on the surface of the fruit surface, limiting oxidation and moisture loss, thereby slowing down the spoilage process.[74] Second, chitosan has antimicrobial properties that allow for inhibiting the growth of micro-organisms responsible for fruit decay.[75] Violacein, on the other hand, acts as an antioxidant, neutralizing the free radicals responsible for the degradation of nutrient compounds and the formation of undesirable compounds.[40] While further studies are still needed for optimizing the applied edible coating, and getting a better understanding on the food preservation, including through antifungal control tests, these preliminary investigations highlight the effectiveness of violacein-containing chitosan coatings in improving food safety and reducing post-harvest losses in the food industry.

Metal sensing of the violacein-containing chitosan films

We have also explored whether these light-sensitive films could also be used for sensing trace metals, such as copper, which can accumulate in food due to agricultural practices or industrial processing.[76] We hypothesized that the well-established photoluminescence properties of violacein could be quenched by trace amounts of copper ions, through electronic or energy transfer from the conjugated functional groups of violacein to the vacant orbitals of the metal. The resulting chemical alteration of the interacting system leads to a loss of violacein photoluminescence, thereby providing a straightforward approach for copper detection.[77] Leveraging on this, we conceived a similar packaging violacein modified film that contains a tiny amount of copper inside, denoted as **CS@Vio^{X}$^{\%}$-Cu$^{1\%}$-*f***. The effect of copper on the violacein photoluminescence could be evidenced by the naked eye, revealing a big discrepancy between copper-containing *versus* copper-free solution and materials (Fig. 8a and c). Measurement of the photoluminescence properties of copper-free **CS@Vio$^{X\%}$-*f*** film *versus* copper-containing film **CS@Vio$^{X\%}$-Cu$^{1\%}$-*f*** provides salient evidence for this quenching, as the typical pattern of violacein entrapping films vanishes (Fig. 8d and Fig. S9, SI). The underlying mechanism for this photoluminescence quenching probably involves the chelation of Cu^{2+} ions with the functional groups of violacein, leading to changes in its electronic structure that diminish its ability to emit light. Potential processes responsible for this quenching include energy transfer, electron transfer or the formation of non-emissive complexes.[78,79] Overall, these results underline the potential of violacein-containing films as promising tools for the detection of copper residues in foods, thereby expanding their utility beyond packaging to food safety and monitoring.

Biodegradability test of violacein-containing chitosan films

Lastly, our tests of the biodegradability reveal the innocuity of violacein introduced in the conceived plastics. Subjecting pristine and violacein-containing chitosan films to preliminary assessment shows that both plastics are prone to decomposition in soil (Fig. 9 and Fig. S10). The pristine chitosan film exhibited the most advanced deterioration, undergoing exten-

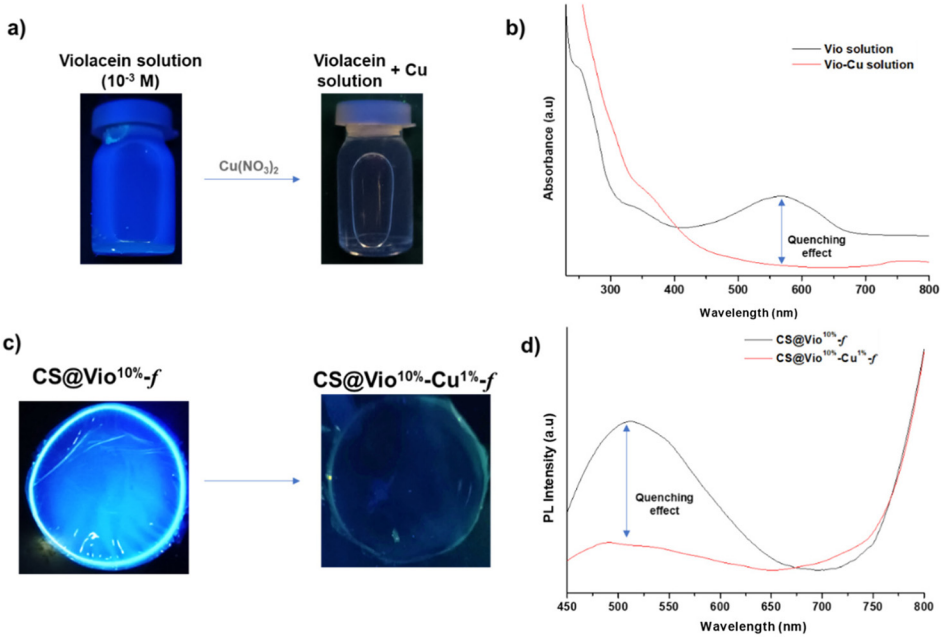

Fig. 8 (a and c) Photoluminescence quenching of violacein solution and **CS@Vio$^{10\%}$-*f*** film under UV light, (b) UV-Vis absorption spectra showing quenching of violacein solution, and (d) photoluminescence quenching of **CS@Vio$^{10\%}$-*f*** film upon interaction with copper ions.

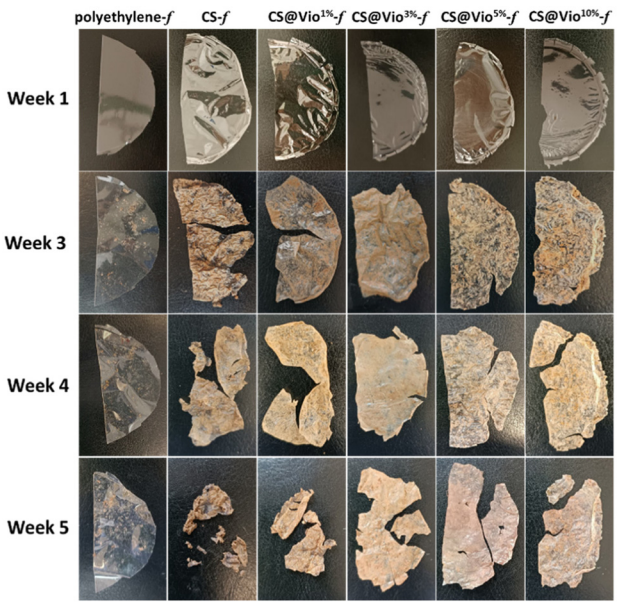

Fig. 9 Biodegradation assessment of **CS@Vio$^{X\%}$-*f*** (*X* = 0, 1, 3, 5 and 10%) films during 5 weeks of biodegradability tests.

sive fragmentation by the fifth week and reaching a degradation level of 72.9%. These findings closely match previous reports showing that chitosan rapidly disintegrates in soil due to enzymatic hydrolysis and microbial assimilation.[80,81] Incorporation of violacein modulated this behavior in a concentration-dependent manner: the film containing one percent violacein remained highly degradable, with a value of 65.1% and visual fragmentation comparable to the pristine sample, whereas higher violacein loadings slowed the decomposition kinetics, leading to degradation levels of 42.2%, 31%, and 25% for the three, five, and ten percent films, respectively. This progressive delay is consistent with the hydrophobicity and antimicrobial character of violacein, which likely reduces water penetration and microbial colonization of the polymer network, thereby limiting enzymatic access within the chitosan matrix. Nonetheless, all violacein-containing films clearly retained their biodegradability, in sharp contrast to the polyethylene control, which remained unchanged over the same period. These results collectively demonstrate that although violacein influences the rate of degradation, it does not compromise the intrinsic eco-responsiveness of chitosan, supporting the potential of these functional films for sustainable applications.

Experimental

Materials

Commercially available reagents and solvents were purchased from Across and Sigma-Aldrich (St Louis, MO, USA). DPPH (2,2-diphenyl-1-picrylhydrazyl) was purchased from Sigma-Aldrich (Hamburg, Germany). Chitosan with an average molecular weight: 100 000–300 000 g mol^{-1}, viscosity: 200–800 cps and degree of deacetylation 75–85%, was purchased from Sigma-Aldrich (Hamburg, Germany) and used for this study. Microorganisms responsible for pathologies such as *S. aureus* ATCC-33591 and *E. coli* ATCC-25922 were used for antibacterial studies.

Production and extraction of violacein

Violacein was produced using an engineered strain of *Y. lipolytica*, JMY7019, kindly provided by the Micalis Institute, INRAE (Jouy-en-Josas, France). The culture protocol was adapted from the corresponding reference with slight modification.[38] A microbial stock (working cell bank) was first prepared by taking a sample aseptically from the agar plate and placed in a 500 ml baffled flask containing the culture medium. The composition of the culture medium was the following: yeast nitrogen base (YNB) without amino acids or ammonium sulfate (1.7 g L^{-1}) and with dextrose (30 g L^{-1}), NH_4Cl (1 g L^{-1}), tryptophan (1 g L^{-1}), leucine (0.2 g L^{-1}), tyrosine (16 mg L^{-1}), phenylalanine (0.2 g L^{-1}), yeast extract (3 g L^{-1}), and saline solution (1×). The composition of the 1000× concentration saline solution was the following: H_3PO_4 85% liquid–107 g, KCl–20 g, NaCl–20 g, $MgSO_4{\cdot}7H_2O$–27 g, $ZnSO_4{\cdot}7H_2O$–7.7 g, $MnSO_4{\cdot}H_2O$–0.47 g, $CoCl_2{\cdot}6H_2O$–0.3 g, $CuSO_4{\cdot}5H_2O$–0.6 g, $Na_2MoO_4{\cdot}2H_2O$–0.094 g, H_3BO–0.3 g, and water up to 1 L. The medium was buffered with 50 mM KH_2PO_4 and Na_2HPO_4 to reach a pH of 6. All the components were prepared separately and sterilized either by autoclaving (20 min at 121 °C for the YNB, dextrose, phenylalanine, leucine, and yeast extract stock solutions) or by filtration, using 0.2 μm nylon filters for the other components to avoid their thermal degradation. Fermentation for microbial stock preparation was conducted for 24 h at 28 °C with shaking at 170 rpm stirring (Thermo Scientific MaxQ 6000, Aubervilliers, France). Cryopreservation of the cells was conducted by adding 1 mL of the culture medium into the cryotubes (VWR, Rosny-sous-Bois, France), in the presence of 1 mL glycerol/water mixture (v : v). The tubes were stored in an ultra-low-temperature freezer at −80 °C (Panasonic MDF-U700VX, Couëron, France).

Violacein production was performed in duplicate in a 1 L baffled Erlenmeyer flask containing 250 mL of the culture medium described above, which was inoculated with 2 mL microbial stock solution. The cultures were then incubated for 168 h at 28 °C and 170 rpm stirring. Microbial biomass was then harvested by centrifugation (Heraeus Multifuge 3 S-R, Villebon-sur-Yvette, France) at 4600 rpm for 15 min and at 4 °C. The supernatants were discarded and violacein was extracted from the wet biomass by adding 96% ethanol (10 : 1 ratio, v : w) into a 200 mL double-jacketed vessel (VRC SAS, Luçon, France), at a constant temperature of 28 °C and stirring at 200 rpm. After 1 h extraction, the mixture was centrifuged at 4600 rpm for 15 min at 4 °C. The supernatant was isolated and the recovered biomass was subjected to two additional extractions under the same conditions. The three supernatants recovered were mixed and ethanol was evaporated to dryness at 60 °C and under reduced pressure. Concentrated violacein was stored at 4 °C and used for the subsequent experiments. The total mass of the crude violacein produced was 300 mg. The extraction yield was evaluated by periodic sampling and quantification, with 92% of the pigment extracted from the initial extraction as discussed in our previous publication.[38] However, the proportion of violacein increased in subsequent extractions. By the third extraction, the pigment load consisted entirely of violacein, highlighting that violacein was the primary component of the crude extract. These findings demonstrate that violacein was effectively concentrated during the extraction process, with increasing purity observed in the later stages.

Preparation of violacein-containing chitosan films (CS@Vio$^{X\%}$-*f*)

Chitosan films entrapping violacein will be denoted as **CS@Vio$^{X\%}$-*f***, with X being the molar ratio of violacein with respect to NH_2 groups of chitosan and (f) is to differentiate films from film-forming coating solution (s) that will be used later (see below).

The following protocol has been used for the preparation of functionalized chitosan films. Firstly, 50 mg of chitosan (CS) was added to 7 ml of a 1% (v/v) aqueous acetic acid solution and stirred for 2 h to obtain a uniform gelled solution. In parallel, a 5.8×10^{-3} M solution of violacein was prepared in ethanol. Once ready, different volumes of this solution were added to the chitosan solution to obtain the desired molar percentage (1%, 3%, 5% and 10%) with respect to NH_2 groups of chitosan, assuming an estimated NH_2 content of 5.8 mmol g^{-1} in the starting biopolymer.[82] After further stirring for 2 h, the resulting solution was poured into Petri dishes and left to dry for 48 h at room temperature. After casting, the dry films were removed from the Petri dishes and subjected to further testing and analysis.

Characterization

FTIR spectra were collected using a SHIMADZU Affinity-1S spectrometer, equipped with an attenuated total reflectance (ATR) accessory. Spectra were captured in the 4000–500 cm^{-1} range, with a resolution of 16 cm^{-1}. A small piece of the film (1 cm × 1 cm piece) was cut and fixed in front of the slot for analysis. A Bruker X-ray AXS D8 Advance diffractometer in Bragg–Brentano configuration, equipped with a LynxEye Super Speed detector, was used for X-ray diffraction (XRD). Diffraction patterns were recorded using Cu Kα radiation (λ = 0.154 nm, 40 kV, 30 mA) in the range from 10 to 80°. A small piece of the film (1 cm × 1 cm piece) was fixed with the support for analysis. UV-visible measurements were carried out using a PerkinElmer Lambda 1050 spectrometer equipped with an integrating sphere. Data were recorded over a wavelength range from 250 to 800 nm in absorbance mode. Both the films and violacein solutions (5.8×10^{-3} M) were analyzed. The films (1 cm × 1 cm piece) were directly placed in the sample holder, while the solutions (3 mL) were measured in standard quartz cuvettes. Photoluminescence measurements were carried out with a FluoroMax-4 spectrofluorometer using FluorEssence software. A 150 W xenon arc lamp was used for excitation, with excitation and emission monochromators fitted with 1200 mm^{-1} groove reflection gratings. These monochromators allowed precise wavelength control, with software-controlled adjustable slits. A small piece of the film (1 cm ×

1 cm piece) was used for such a purpose and placed on a rotating support tilted at 30° before measurement. Scanning electron microscopy (SEM) images were obtained using a JEOL JSM 6700F with an accelerating voltage of 12 kV and a magnification level of 2000. A small piece of the film (1 cm × 1 cm piece) was coated with a thin layer of gold using a Denton Vacuum model DESK II sputter and fixed on the top for visualization. An automatic contact angle system (OCA 40, DATAPHYSICS) was used to assess the hydrophobicity of the as-prepared films. To do this, a 1 cm × 1 cm piece of film was placed on a horizontal platform inside the system. A drop of 10 μl of distilled water was applied to the film surface, and the contact angle was measured to assess the hydrophobic properties of the surface. The film thickness was measured at five points using a Mitutoyo digital caliper (precision: 0.001 mm), and the average value was used. The film density was calculated from the specimen's weight and volume, with the volume determined by the area and thickness.[83] Thermogravimetric analysis (TGA) was performed under a nitrogen atmosphere at a heating rate of 10 °C min^{-1}, covering a temperature range from room temperature to 700 °C, using a TGA Discovery analyzer (TA Instruments, New Castle, DE, USA). For each measurement, approximately 10 mg of the sample was cut and placed into a platinum pan at room temperature, and its weight degradation was monitored by increasing the temperature until 700 °C.

Water solubility (WS) and water vapor permeability (WVP). Water solubility (WS) of the films was assessed by first weighing pre-dried samples (2 cm × 2 cm, dried at 80 °C for 24 h), and then immersing them in 30 ml of deionized water at room temperature for 24 h. After immersion, the films were removed, dried again at 80 °C for 24 h, and weighed. The WS was then calculated using eqn (1).[84] Next the WVP was determined using the ASTM E96/E96M method with slight modifications.[85] Samples were placed on the circular orifices of cells containing 4 g of anhydrous calcium chloride $CaCl_2$ (0% relative humidity) and incubated at 50% RH and 32 °C. The weight of the permeation cells was measured six times over 6 hours to calculate the water vapor transmission coefficient (WVT) and the WVP was then calculated using eqn (2)

$$\mathrm{WS}\,(\%) = \frac{W_0 - W_1}{W_0} \times 100 \quad (1)$$

$$\mathrm{WVP} = \frac{\mathrm{WVT}}{\Delta P}\xi = \frac{\mathrm{WVT}}{P(R_1 - R_2)}\xi. \quad (2)$$

Here, ξ represents the thickness of the film, while P is the vapor pressure at the test temperature of 25 °C. The values of R_1 and R_2 correspond to the relative humidity inside the glass bottle (0%) and the climatic chamber (50%), respectively.

Mechanical properties. Mechanical properties of the films were evaluated, including tensile strength (TS), which reflects the material's resistance to breaking under tension, Young's modulus (YM), which indicates the film's rigidity and elongation at break (EB), which measures its flexibility. These parameters were measured using an Instron universal testing machine (model 5565, Instron Engineering Corporation, Canton, MA, USA). Rectangular film samples (1 cm × 40 cm) were clamped between two 1000 N load cells and stretched at a speed of 5 mm min^{-1}. The reported values represent the average of three repeated measurements.[86]

Antioxidant activity and total phenolic content (TPC). The antioxidant activity of the manufactured films was assessed using the DPPH free radical scavenging test.[87] First, 25 mg of each film was dissolved in 3 ml of methanol and left in contact for 20 min (solution 1). Simultaneously, a reference solution (solution 2) was prepared by dissolving 4.0 mg DPPH in 100 ml methanol and stirring the mixture for 30 min; then its absorbance was measured at 515 nm (A_{ref}). Next, 1.5 ml of solution 1 was mixed with 3 ml of solution 2, followed by vigorous stirring. After incubation at room temperature in the dark for 30 min, the absorbance of the mixture (A_{sample}) was measured at 515 nm. Antioxidant activity (OA %) was calculated according to eqn (3):

The total phenolic content of chitosan-based films was determined using the Folin–Ciocalteu colorimetric method with slight modifications.[88] Gallic acid solutions ranging from 0 to 15 μg ml^{-1} were used to create a calibration curve. To prepare the film extract, 12.5 mg of the film sample was soaked in 1.5 ml of distilled water for 24 hours. Then, 0.1 ml of the extract was mixed with 6 ml of distilled water and 0.5 ml of Folin–Ciocalteu reagent. After 8 minutes, 1.5 ml of 10 wt% sodium carbonate solution was added, and the mixture was brought to a total volume of 10 ml with distilled water. Then it was incubated in the dark at room temperature for 2 hours, followed by absorbance measurement at 765 nm using a UV spectrophotometer. The TPC was expressed as gallic acid equivalents (GAE), calculated as the amount of gallic acid in mg per gram of dry sample weight using eqn (4).

$$\mathrm{OA}\,(\%) = \frac{A_{ref} - A_{sample}}{A_{ref}} \times 100 \quad (3)$$

$$\mathrm{Abs}_{765} = 0.036\ \text{mg gallic acid} - 0.1134. \quad (4)$$

Antibacterial activity. The antibacterial activity of violacein-enriched chitosan films was evaluated using two methods: the total viable colony count method and the disc diffusion method.[89,90] Two common foodborne pathogenic bacteria, *E. coli* (Gram-negative) and *S. aureus* (Gram-positive), were subjected to this evaluation. Bacteria were inoculated using a sterile inoculating loop into 20 ml of tryptic soy broth (TSB) and brain heart infusion (BHI) broth respectively, and then incubated at 37 °C for 16 h. Next, a 10 ml volume of diluted broth (containing between 10^4 and 10^6 CFU ml^{-1}) was added to a 50 ml conical flask, into which 25 mg film samples were placed. This solution was incubated at 37 °C for 12 h with gentle agitation. A control experiment was carried out using a flask containing only the diluted broth, with no film samples added. At intervals of 3, 6, 9 and 12 h incubation, the total number of viable colonies (expressed as log 10 CFU mL^{-1}) was counted for each pathogen by growing the samples on agar plates. This procedure was repeated three times at each time

interval. In addition, the disc diffusion method was employed, in which film samples were cut into 5 mm circles and placed on Mueller-Hinton agar plates inoculated with *S. aureus* and *E. coli* at a bacterial density of approximately 1.5×10^6 CFU mL^{-1}. The plates were incubated at 37 °C for 24 hours, and the diameters of the inhibition zones around the discs were measured to assess the antibacterial activity.

Biodegradability test of violacein-containing chitosan films. The biodegradability of violacein-containing chitosan films was evaluated using soil microorganisms. The test was carried out on a laboratory scale, following the methodology outlined by Wronska *et al.*, with some modifications.[80] Soil samples were collected from the garden of Euromed University in Fes, Morocco, and served as the incubation medium. The soil was kept at room temperature with 70% moisture and a pH of 6. The soil was placed into a specialized container, and samples were buried at a depth of approximately 7 cm, each in a separate container, and incubated at room temperature. The samples were retrieved at different time intervals (3, 4, and 5 weeks of incubation) and gently brushed to remove any soil residues, and then photographed. In the final week, the samples were gently washed with distilled water, dried at 50 °C for 4 hours, and weighed, and the percentage of degradation (PD) was calculated as follows:

$$\mathrm{PD}\,(\%) = \frac{W_\mathrm{i} - W_\mathrm{f}}{W_\mathrm{i}} \times 100. \quad (5)$$

Color parameters. Color parameters (L^* for brightness, a^* for red–green, and b^* for yellow–blue) of the films were measured using a Konica Minolta CM-5 spectrophotometer, under CIE Standard Illuminant D65 and a 10° standard observer. The total color difference (ΔE) was calculated using eqn (6):

$$\Delta E = \sqrt{\Delta L^{*2} + \Delta a^{*2} + \Delta b^{*2}}. \quad (6)$$

Food coating process

To evaluate their performance, different spray solutions of chitosan, violacein, and their combination **CS@Vio$^{10\%}$-*s*** were prepared and applied as coating on three types of fruit purchased from a local market, with different shelf lives: strawberries, blueberries and raspberries. The method used for this evaluation was that of edible coating.[91] Hydrogel solutions (35 ml) were prepared as follows:

CS-s. 250 mg of chitosan (CS) was added to 35 ml of a 1% (v/v) aqueous acetic acid solution and stirred for 2 h to obtain a uniform gelled solution.

Vio-s. A violacein solution (5.8×10^{-3} M) was prepared by dissolving the compound in ethanol to a final volume of 35 mL.

CS@Vio$^{10\%}$-s. The two solutions were mixed by adding 12.5 mL of **Vio-*s*** to 35 mL of **CS-*s***, resulting in a mixture containing 10% violacein relative to the amine functional groups of chitosan.

For each formulation, fruit samples were coated using a successive dip-coating technique. Each fruit was immersed several times until the film uniformly adhered to the entire surface, and then withdrawn and left to dry at room temperature. After coating, the remaining solution was measured to determine the exact amount of solution that was applied to the fruit. An untreated control sample was also prepared for comparison. After coating, the fruit was stored for 10 days at ambient temperature and humidity. Film performance was evaluated based on retention of fruit appearance, color and texture, as well as resistance to deterioration.

Metal sensing. A quenching test was used to study the interaction between copper ions and violacein as a way of sensing metal contaminants, which can accumulate in foods as a result of agricultural practices or industrial processes. For this purpose, a solution of violacein (20 ml, 10^{-3} mol l^{-1}) was prepared and mixed with 2 ml of a solution of copper nitrate (10^{-3} mol l^{-1}) to observe the direct effect of copper ions on the photoluminescence properties of violacein. Next, 1% copper residue was incorporated within violacein-containing chitosan films featuring 10% of violacein pigment and prepared as follows:

CS@Vio$^{10\%}$-Cu$^{1\%}$-f. 7 mL of **CS-*s*** aqueous acetic acid solution 1% (v/v) was mixed with 2.5 mL of **Vio-*s*** (5.8×10^{-3} M) ethanol solution and 2 mL of a (3.9×10^{-3} M) $Cu(NO_3)_2$ aqueous solution to prepare a composite formulation containing violacein and 1% copper. After further stirring for 2 h, the resulting solution was poured into Petri dishes and left to dry for 48 h at room temperature. After casting, the dry film was removed from the Petri dishes. The photoluminescence properties of the solution and films were characterized before and after exposure to copper ions to unveil the possible metal quenching caused by violacein.

Statistical analysis. The difference between factors and levels was evaluated using analysis of variance (ANOVA). Tukey's test was applied to compare means and identify significantly different groups ($p < 0.05$). Data were processed using Jamovi software, and the results are presented as mean ± standard deviation.

Conclusions

Sustainable coating and packaging materials derived from bio-based resources are gaining increasing attention as viable alternatives to conventional petroleum-based plastics, offering enhanced food preservation, safety, and quality monitoring. In this work, we successfully combined two environmentally benign components: chitosan, a naturally occurring biopolymer obtained from shellfish waste, and violacein extracts, a biotechnologically-engineered pigment toward the development of multifunctional food packaging films. The incorporation of the hydrophobic violacein moiety proved compatible with the chitosan gel-forming system, enabling the fabrication of transparent, flexible films with improved mechanical strength, thereby replacing the use of costly synthesized nano-

metric fillers and plasticizers, while providing additional light-responsive functionalities, including photoluminescence and UV-shielding effects. Moreover, violacein-containing chitosan films exhibited enhanced antioxidant and antibacterial activities, contributing to the effective extension of the food shelf life. These films also demonstrated smart sensing capability, exemplified by the visual detection of residual copper contamination. Overall, the interfacial interplay of violacein and chitosan provides promising and cost-effective platform hydrogels for sustainable food packaging, with potential applications extending to green adhesives, biomedical devices, electronics, and cosmetics, owing to their intrinsic biocompatibility and environmental friendliness.

Conflicts of interest

There are no conflicts to declare.

Data availability

The data supporting this article have been included as part of the supplementary information (SI). Supplementary information is available. See DOI: https://doi.org/10.1039/d6lp00065g.

Acknowledgements

Hassan II Academy of Science and Technology is acknowledged for the financial support of the Nano-Bio-Mat project. UEMF is acknowledged for facilities.

References

1 J. H. Clark, T. J. Farmer, L. Herrero-Davila and J. Sherwood, *Green Chem.*, 2016, **18**, 3914–3934.
2 J. Sherwood, *Bioresour. Technol.*, 2020, **300**, 122755.
3 B. Ates, S. Koytepe, A. Ulu, C. Gurses and V. K. Thakur, *Chem. Rev.*, 2020, **120**, 9304–9362.
4 C. Xu, M. Nasrollahzadeh, M. Selva, Z. Issaabadi and R. Luque, *Chem. Soc. Rev.*, 2019, **48**, 4791–4822.
5 Y. Cho, P. T. T. Ninh, S. Hwang, S. Choe and J. Myung, *ACS Mater. Lett.*, 2025, **7**, 1563–1592.
6 D. Schieppati, N. A. Patience, F. Galli, P. Dal, I. Seck, G. S. Patience, D. Fuoco, X. Banquy and D. C. Boffito, *Ind. Eng. Chem. Res.*, 2023, **62**, 12757–12794.
7 R. A. Sequeira, D. Mondal and K. Prasad, *Green Chem.*, 2021, **23**, 8821–8847.
8 E. Lizundia, F. Luzi and D. Puglia, *Green Chem.*, 2022, **24**, 5429–5459.
9 N. V. Veríssimo, C. U. Mussagy, A. A. Oshiro, C. M. N. Mendonça, V. de Carvalho Santos-Ebinuma, A. Pessoa, R. P. de Souza Oliveira and J. F. B. Pereira, *Green Chem.*, 2021, **23**, 9377–9400.
10 W. Levasseur, P. Perré and V. Pozzobon, *Biotechnol. Adv.*, 2020, **41**, 107545.
11 T. Maschmeyer, R. Luque and M. Selva, *Chem. Soc. Rev.*, 2020, **49**, 4527–4563.
12 M. Beaumont, R. Tran, G. Vera, D. Niedrist, A. Rousset, R. Pierre, V. P. Shastri and A. Forget, *Biomacromolecules*, 2021, **22**, 1027–1052.
13 V. Venugopal, A. Sasidharan and T. Rustad, *J. Agric. Food Chem.*, 2023, **71**, 17494–17509.
14 N. Yan and X. Chen, *Nature*, 2015, **524**, 155–157.
15 I. Younes and M. Rinaudo, *Mar. Drugs*, 2015, **13**, 1133–1174.
16 X. Chen, H. Yang and N. Yan, *Chem. – Eur. J.*, 2016, **22**, 13402–13421.
17 C. Meredith, *Chem. Rev.*, 2022, **122**, 15993–15995.
18 M. R. Kumar, R. A. Muzzarelli, C. Muzzarelli, H. Sashiwa and A. Domb, *Chem. Rev.*, 2004, **104**, 6017–6084.
19 H. Amiri, M. Aghbashlo, M. Sharma, J. Gaffey, L. Manning, S. M. Moosavi Basri, J. F. Kennedy, V. K. Gupta and M. Tabatabaei, *Nat. Food*, 2022, **3**, 822–828.
20 S. Takeshita, S. Zhao, W. J. Malfait and M. M. Koebel, *Angew. Chem., Int. Ed.*, 2021, **60**, 9828–9851.
21 S. Ladet, L. David and A. Domard, *Nature*, 2008, **452**, 76–79.
22 A. El Kadib, *Chem. Rec.*, 2020, **20**, 753–772.
23 H. Wang, J. Qian and F. Ding, *J. Agric. Food Chem.*, 2018, **66**, 395–413.
24 F. N. Maluin, *ACS Agric. Sci. Technol.*, 2024, **4**, 1136–1162.
25 S. Sarkar, S. Manna, S. Das, S. De, P. Paul, T. K. Dua, R. Sahu and G. Nandi, *ACS Food Sci. Technol.*, 2023, **3**, 1877–1889.
26 I. Leceta, P. Guerrero, S. Cabezudo and K. de la Caba, *J. Cleaner Prod.*, 2013, **41**, 312–318.
27 A. El Kadib, N. Wrońska, K. Lisowska, A. Anouar, N. Katir, K. Miłowska, B. Bielska and M. Bryszewska, in *Functional Materials in Biomedical Applications*, Jenny Stanford Publishing, 2023, pp. 1–50.
28 Y. Guo, D. Qiao, S. Zhao, B. Zhang and F. Xie, *Prog. Polym. Sci.*, 2024, 101872.
29 P. Sahariah and M. Másson, *Biomacromolecules*, 2017, **18**, 3846–3868.
30 S. Manna, A. Seth, P. Gupta, G. Nandi, R. Dutta, S. Jana and S. Jana, *ACS Biomater. Sci. Eng.*, 2023, **9**, 2181–2202.
31 M. I. Wahba, *J. Biomater. Sci., Polym. Ed.*, 2020, **31**, 350–375.
32 A. R. Karimi and A. Khodadadi, *ACS Appl. Mater. Interfaces*, 2016, **8**, 27254–27263.
33 C. Espro, E. Paone, F. Mauriello, R. Gotti, E. Uliassi, M. L. Bolognesi, D. Rodríguez-Padrón and R. Luque, *Chem. Soc. Rev.*, 2021, **50**, 11191–11207.
34 C. Huang, X. Chu, W. Hui, C. Xie and X. Xu, *Biotechnol. Appl. Biochem.*, 2023, **70**, 1582–1596.
35 C. Sánchez, A. F. Braña, C. Méndez and J. A. Salas, *ChemBioChem*, 2006, **7**, 1231–1240.
36 M. Kholany, P. Trébulle, M. Martins, S. P. Ventura, J. M. Nicaud and J. A. Coutinho, *J. Chem. Technol. Biotechnol.*, 2020, **95**, 1126–1134.

37 D. Chelminiak-Dudkiewicz, M. Wujak, D. T. Mlynarczyk, J. Dlugaszewska, K. Mylkie, A. Smolarkiewicz-Wyczachowski and M. Ziegler-Borowska, *Heliyon*, 2024, **10**.
38 G. Nemer, N. Louka, P. Rabiller Blandin, R. G. Maroun, E. Vorobiev, T. Rossignol, J.-M. Nicaud, E. Guénin and M. Koubaa, *Molecules*, 2023, **28**, 4292.
39 I. Rivero Berti, B. E. Rodenak-Kladniew, S. F. Katz, E. C. Arrua, V. A. Alvarez, N. Duran and G. R. Castro, *Front. Chem.*, 2022, **10**, 914126.
40 I. R. Berti, B. Rodenak-Kladniew, A. A. Perez, L. Santiago, N. Duran and G. R. Castro, *React. Funct. Polym.*, 2019, **136**, 122–130.
41 J. Chabbi, O. Jennah, N. Katir, M. Lahcini, M. Bousmina and A. El Kadib, *Carbohydr. Polym.*, 2018, **183**, 287–293.
42 J. Chabbi, A. Aqil, N. Katir, B. Vertruyen, C. Jerôme, M. Lahcini and A. El Kadib, *Carbohydr. Polym.*, 2020, **230**, 115634.
43 L. Marin, S. Moraru, M. C. Popescu, A. Nicolescu, C. Zgardan, B. C. Simionescu and M. Barboiu, *Chem. – Eur. J.*, 2014, **20**, 4814–4821.
44 N. Hammi, M. Kędzierska, N. Wrońska, N. Katir, J. Dhainaut, S. Royer, K. Lisowska, M. Bryszewska, K. Miłowska and A. El Kadib, *Mater. Adv.*, 2023, **4**, 5191–5199.
45 S. Y. Choi, S. Lim, G. Cho, J. Kwon, W. Mun, H. Im and R. J. Mitchell, *Environ. Microbiol.*, 2020, **22**, 705–713.
46 I. Rivero Berti, M. E. Gantner, S. Rodriguez, G. A. Islan, W. J. Fávaro, A. Talevi, G. R. Castro and N. Durán, *Front. Nanotechnol.*, 2023, **5**, 1186386.
47 M. Bousmina, *Macromolecules*, 2006, **39**, 4259–4263.
48 S. S. Ray and M. Okamoto, *Prog. Polym. Sci.*, 2003, **28**, 1539–1641.
49 A. M. P. Anahas, S. Kumaran, M. Kandeel, G. Muralitharan, J. Silviya, G. L. Adhimoolam, M. Panagal, S. R. Pugazhvendan, G. Suresh, A. Wilson, S. Rethinam and P. Nainangou, *J. Nanomater.*, 2022, 3885396.
50 W. A. Ahmad, W. Y. W. Ahmad, Z. A. Zakaria and N. Z. Yusof, in *Application of Bacterial Pigments as Colorant: The Malaysian Perspective*, ed. W. A. Ahmad, W. Y. Wan Ahmad, Z. A. Zakaria and N. Z. Yusof, Springer Berlin Heidelberg, Berlin, Heidelberg, 2012, pp. 25–44. DOI: 10.1007/978-3-642-24520-6_2.
51 A. A. Beckstead, Y. Zhang, J. K. Hilmer, H. J. Smith, E. Bermel, C. M. Foreman and B. Kohler, *J. Phys. Chem. B*, 2017, **121**, 7855–7861.
52 C. Dantas, P. L. Volpe, N. Durán and M. Ferreira, *J. Braz. Chem. Soc.*, 2012, **23**, 2054–2064.
53 C. Dantas, R. Tauler and M. M. C. Ferreira, *Anal. Bioanal. Chem.*, 2013, **405**, 1293–1302.
54 X. Sun, J. Wang, M. Dong, H. Zhang, L. Li and L. Wang, *Trends Food Sci. Technol.*, 2022, **119**, 122–132.
55 M. Hasani, F. Wu and K. Warriner, *J. Food Sci.*, 2020, **85**, 2645–2655.
56 M. A. Sani, A. Khezerlou, M. Tavassoli, A. H. Abedini and D. J. McClements, *Trends Food Sci. Technol.*, 2024, 104366.
57 M. Konzen, D. De Marco, C. A. Cordova, T. O. Vieira, R. V. Antonio and T. B. Creczynski-Pasa, *Bioorg. Med. Chem.*, 2006, **14**, 8307–8313.
58 W. Cao, W. Chen, S. Sun, P. Guo, J. Song and C. Tian, *J. Mol. Struct.: THEOCHEM*, 2007, **817**, 1–4.
59 W. Liu, J. Xie, L. Li, B. Xue, X. Li, J. Gan, Z. Shao and T. Sun, *J. Mol. Struct.*, 2021, **1239**, 130531.
60 Z. Si, Z. Hou, Y. S. Vikhe, K. R. V. Thappeta, K. Marimuthu, P. P. De, O. T. Ng, P. Li, Y. Zhu and K. Pethe, *ACS Appl. Mater. Interfaces*, 2021, **13**, 3237–3245.
61 A. Guarnieri, M. Triunfo, C. Scieuzo, D. Ianniciello, E. Tafi, T. Hahn, S. Zibek, R. Salvia, A. De Bonis and P. Falabella, *Sci. Rep.*, 2022, **12**, 8084.
62 G. M. de Oca-Vásquez, M. Esquivel-Alfaro, J. R. Vega-Baudrit, G. Jiménez-Villalta, V. H. Romero-Arellano and B. Sulbarán-Rangel, *J. Agric. Food Res.*, 2023, **14**, 100759.
63 O. Dardari, O. Amadine, Y. Essamlali, S. Sair, S. Aboulhrouz, H. Maati, G. Achagri and M. Zahouily, *J. Inorg. Organomet. Polym. Mater.*, 2022, **32**, 4304–4319.
64 N. Wrońska, N. Katir, K. Miłowska, N. Hammi, M. Nowak, M. Kędzierska, A. Anouar, K. Zawadzka, M. Bryszewska and A. El Kadib, *Int. J. Mol. Sci.*, 2021, **22**, 5839.
65 L. L. Cazoto, D. Martins, M. G. Ribeiro, N. Durán and G. Nakazato, *J. Antibiot.*, 2011, **64**, 395–397.
66 K.-C. Cheng, H.-C. Hsiao, Y.-C. Hou, C.-W. Hsieh, H.-Y. Hsu, H.-Y. Chen and S.-P. Lin, *Antioxidants*, 2022, **11**, 849.
67 N. Durán, G. Nakazato, M. Durán, I. R. Berti, G. R. Castro, D. Stanisic, M. Brocchi, W. J. Fávaro, C. V. Ferreira-Halder and G. Z. Justo, *World J. Microbiol. Biotechnol.*, 2021, **37**, 151.
68 M. Kanelli, M. Mandic, M. Kalakona, S. Vasilakos, D. Kekos, J. Nikodinovic-Runic and E. Topakas, *Front. Microbiol.*, 2018, **9**, 1495.
69 J. Lee, J. Bae, D.-Y. Youn, J. Ahn, W.-T. Hwang, H. Bae, P. K. Bae and I.-D. Kim, *Chem. Eng. J.*, 2022, **444**, 136460.
70 B. Chatterjee, J. B. Aswathanarayan and R. R. Vittal, *J. Packag. Technol. Res.*, 2022, **6**, 101–114.
71 S. Parvez and I. A. Wani, in *Postharvest Biology and Technology of Temperate Fruits*, ed. S. A. Mir, M. A. Shah and M. M. Mir, Springer International Publishing, Cham, 2018, pp. 331–348. DOI: 10.1007/978-3-319-76843-4_14.
72 H. M. Ooi, M. H. Munawer and P. L. Kiew, *AIP Conf. Proc*, 2023, 2785.
73 A. Quintanilla, A. Mencia, J. Powers, B. Rasco, J. Tang and S. S. Sablani, *Drying Technol.*, 2022, **40**, 299–309.
74 R. Eldib, E. Khojah, A. Elhakem, N. Benajiba and M. Helal, *Coatings*, 2020, **10**, 962.
75 T. Liu, J. Li, Q. Tang, P. Qiu, D. Gou and J. Zhao, *Foods*, 2022, **11**, 1490.
76 K. A. Kirk and S. Andreescu, *Anal. Chem.*, 2019, **91**, 13892–13899.
77 Y.-X. Sun, Y.-G. Sun, Z.-P. Deng, Y.-H. Jia, W.-Y. Han, J.-J. Wang and Y. Sun, *J. Mol. Struct.*, 2023, **1291**, 136069.

78 Z.-C. Liu, Z.-Y. Yang, T.-R. Li, B.-D. Wang, Y. Li, D.-D. Qin, M.-F. Wang and M.-H. Yan, *Dalton Trans.*, 2011, **40**, 9370–9373.
79 T. Wu, S. Jiang, P. N. Samanta, Y. Xie, J. Li, X. Wang, M. Devashis, X. Gu, Y. Wang and W. Huang, *Chem. Commun.*, 2020, **56**, 12057–12060.
80 N. Wrońska, N. Katir, M. Nowak-Lange, A. El Kadib and K. Lisowska, *Foods*, 2023, **12**, 3519.
81 J. M. F. Pavoni, N. Z. dos Santos, I. C. May, L. D. Pollo and I. C. Tessaro, *Polym. Bull.*, 2021, **78**, 981–1000.
82 M. Boundor, B. Bielska, N. Katir, N. Wrońska, K. Lisowska, M. Bryszewska, K. Miłowska and A. El Kadib, *ACS Appl. Polym. Mater.*, 2023, **5**, 9952–9963.
83 L. Wang, Y. Dong, H. Men, J. Tong and J. Zhou, *Food Hydrocoll.*, 2013, **32**, 35–41.
84 M. Kaya, S. Khadem, Y. S. Cakmak, M. Mujtaba, S. Ilk, L. Akyuz, A. M. Salaberria, J. Labidi, A. H. Abdulqadir and E. Deligöz, *RSC Adv.*, 2018, **8**, 3941–3950.
85 O. Dardari, M. A. Benzaouia, A. El Idrissi, B.-E. Channab, G. R. Benjellound, A. El Gharrak, M. El Ouardi and A. El Kadib, *Int. J. Biol. Macromol.*, 2025, 143213.
86 Y. Xu, X. Liu, Q. Jiang, D. Yu, Y. Xu, B. Wang and W. Xia, *Carbohydr. Polym.*, 2021, **260**, 117778.
87 M. Alizadeh-Sani, M. Tavassoli, E. Mohammadian, A. Ehsani, G. J. Khaniki, R. Priyadarshi and J.-W. Rhim, *Int. J. Biol. Macromol.*, 2021, **166**, 741–750.
88 U. Siripatrawan and B. R. Harte, *Food Hydrocoll.*, 2010, **24**, 770–775.
89 J. C. Antunes, T. D. Tavares, M. A. Teixeira, M. O. Teixeira, N. C. Homem, M. T. P. Amorim and H. P. Felgueiras, *Pharmaceutics*, 2021, **13**, 195.
90 J. Jiang, X. Chen, G.-L. Zhang, H. Hao, H.-M. Hou and J. Bi, *Carbohydr. Polym.*, 2022, **285**, 119234.
91 A. A. Wardana, A. Koga, F. Tanaka and F. Tanaka, *Sci. Rep.*, 2021, **11**, 18412.